Biological Relevance of a Stable Biochemical Interaction between the Tombusvirus-Encoded P19 and Short Interfering RNAs

Rustem Omarov,[1] Kim Sparks,[1] Lindsay Smith,[1] Jelena Zindovic,[1]† and Herman B. Scholthof[1,2]*

*Department of Plant Pathology and Microbiology[1] and Intercollegiate Faculty of Virology,[2]
Texas A&M University, 2132 TAMU, College Station, Texas 77843*

The *Tomato bushy stunt virus* (TBSV)-encoded *p19* protein (P19) is widely used as a robust tool to suppress RNA interference (RNAi) in various model organisms. P19 dimers appropriate 21-nucleotide (nt) duplex short interfering RNAs (siRNAs) generated by Dicer presumably to prevent programming of the RNA-induced silencing complex (RISC). In the context of virus infection, this model predicts that P19 mutants compromised for siRNA binding cannot prevent RISC-mediated degradation of TBSV RNA and thus reduce viral pathogenicity. To test this, we used P19/43 (R→W), which is less pathogenic than wild-type P19 (wtP19), and P19/75-78 (RR→GG), with pathogenicity properties (i.e., viral spread and symptom induction) comparable to those of a P19-null mutant. We demonstrate that P19/43 still suppresses RNAi-mediated viral RNA degradation in infected *Nicotiana benthamiana*, while P19/75-78 is unable to prevent this clearance of viral RNA, leading to an irreversible recovery phenotype. Gel filtration and immunoprecipitation assays show that at the onset of the infection, wtP19, P19/43, and P19/75-78 readily accumulate, and they form dimers. The wtP19 is stably associated with duplex ~21-nt TBSV siRNAs, while P19/75-78 does not bind these molecules, and the electrostatic interaction of P19/43 with siRNAs is perturbed for ~21-nt duplexes but not for longer siRNAs. This is the first clear demonstration of a direct correlation between a novel structurally orchestrated siRNA binding of an RNAi suppressor and its roles in viral pathogenesis. The findings should be particularly valuable for the RNAi field in general because the P19 mutants enable precise determination of siRNA appropriation effects.

RNA interference (RNAi) is a posttranscriptional RNA silencing process that is evolutionary conserved across eukaryotic kingdoms to regulate the levels of specific RNAs during development. RNAi also functions as a host defense system against virus infections, as was first shown for plant viruses (1). As a countermeasure, viruses have evolved suppressors of gene silencing (15, 26, 27, 32, 38). One of the biochemically best characterized suppressors is a protein of 19 kDa (P19) encoded by *Tomato bushy stunt virus* (TBSV) and related tombusviruses that is functional as a suppressor in several model systems (4, 12, 13, 40, 41).

During TBSV replication in plants, abundant levels of highly structured genomic single-stranded RNA (ssRNA) and double-stranded RNAs (dsRNAs) accumulate that potentially form excellent substrates for one of the first steps in RNAi: Dicer-mediated cleavage of dsRNAs into duplex short interfering RNAs (siRNAs) (2, 19, 20, 43). In a subsequent step of RNAi, these ds-siRNAs unwind to donate one of the siRNA strands to the RNA-induced silencing complex (RISC). This forms the catalytic entity for RNA degradation that uses the incorporated siRNA to specifically target complementary RNAs (7–9, 14, 16, 17). However, suppressors of RNAi, like P19, can interfere with this process (10, 33).

The X-ray crystallographic structure of the P19-siRNA complex (37, 42) revealed an elegant structural conformation whereby caliper tryptophan residues on P19 dimers precisely measure the binding of 21-nucleotide (nt) siRNAs by P19 dimers; these siRNA duplexes have 2-nt 3′ overhangs. The association between P19 and siRNAs has also been shown to occur in infected plants (10, 12), and the virus-derived siRNAs predominantly map to structured regions scattered across the genome (18). Our current working model is that during TBSV infection of plants, P19 appropriates abundantly circulating TBSV-specific siRNAs, thereby rendering these unavailable to program the RISC, to prevent degradation of viral RNA and thus permit its maintenance for systemic invasion.

To determine whether siRNA binding by P19 directly and strictly correlates with RNA maintenance and pathogenicity, we selected two TBSV P19 amino acid substitution mutants that we previously had analyzed for their biological properties (5) as the basis for the present study. The first mutant has both Arg residues at positions 75 and 78 substituted for Gly (P19/75-78), and this severely compromises its pathogenic roles in systemic spread and symptom induction. Here we demonstrate that P19/75-78 accumulates to levels comparable to those of wild-type P19 (wtP19) and forms dimers, yet it is specifically compromised for binding to TBSV-derived siRNAs in *Nicotiana benthamiana*, and this abolishes its ability to protect viral RNA in infected plants, leading to a recovery phenotype. The recovery phenotype cannot be reversed by superinfection with TBSV expressing wtP19, suggesting that P19 can prevent but not reverse programming of RISC.

The second mutant (P19/43; Arg43→Trp) was selected because its pathogenic properties during infection are interme-

* Corresponding author. Mailing address: Department of Plant Pathology and Microbiology, Texas A&M University, 2132 TAMU, College Station, TX 77843. Phone: (979) 862-1495. Fax: (979) 845-6483. E-mail: herscho@tamu.edu.
† Present address: Department of Plant Protection, Biotechnical Institute, University of Montenegro, 81000 Podgorica, Serbia and Montenegro.

diate compared to those of infections in the presence of wtP19 or absence of P19 (5). The perceived biochemical importance of Arg43 was also based on the observation that this amino acid is highly conserved among tombusviruses (37). We show that, although P19/43 suppresses viral RNA degradation in *N. benthamiana*, the stability of the interaction between P19/43 dimers and siRNAs is noticeably perturbed. This correlates with its milder symptom phenotype and a diminished capacity to promote systemic spread in some hosts.

Our results provide the first clear evidence for a structurally directed role of P19 in tenaciously capturing and binding siRNAs during virus infection and thus abrogate programming of an antiviral RISC that could otherwise compromise the establishment or maintenance of a systemic invasion. The findings should be of immediate value to various disciplines because the non-sequence-specific siRNA binding activity of P19 has been shown to operate in several systems and the mutants provide unique tools to precisely control siRNA binding in RNAi studies in vitro and in various model organisms.

MATERIALS AND METHODS

Inoculation and analysis of plants. In vitro-generated transcripts of full-length cDNAs expressing wtP19 (pTBSV-100) (11), no P19 (pHS157), P19/75-78, and P19/43 (5) were prepared essentially as described previously (11). In short, the plasmids (1 µg) were linearized at the 3′ terminus of the viral sequence by digestion with SmaI, and transcripts were made with T7 RNA polymerase. *N. benthamiana* plants were inoculated by standard procedures (29).

RNA analysis. Total RNA was extracted by grinding of ~200 mg of leaf material (inoculated or systemically infected leaves) on ice in 1 ml of extraction buffer (100 mM Tris-HCl, pH 8.0, 1 mM ETDA, 0.1 M NaCl, 1% sodium dodecyl sulfate [SDS]). Samples were immediately extracted twice with phenol-chloroform (1:1 [vol/vol]) at room temperature and precipitated with 8 M lithium chloride solution (1:1 [vol/vol]) at 4°C for 1 h. The resulting pellets were washed with 70% ethanol and then resuspended in RNase-free distilled water and used for Northern blot hybridization. Approximately 10 µg of total plant RNA was separated in 1% agarose gels and transferred to nylon membranes (Osmonics, Westborough, MA). TBSV genomic RNA (gRNA) and subgenomic RNAs (sgRNAs) were detected by hybridization with [^{32}P]dCTP-labeled TBSV-specific probes, essentially as previously described (29).

Sephacryl S-200 fractionation. Two grams of infected *N. benthamiana* leaf tissue was homogenized in extraction buffer (200 mM Tris-HCl, pH 7.4, 5 mM dithiothreitol [DTT]). The plant extracts were filtered through cheesecloth and then centrifuged for 15 min at 14,000 × *g* at 4°C. The supernatant (1.5 ml) was loaded and fractionated on a column (2.5 cm in diameter by 80 cm in length) packed with Sephacryl S-200 High Resolution (Amersham, Piscataway, NJ) at a flow rate of 1.3 ml/min. The column was pre-equilibrated with elution buffer (50 mM Tris-HCl, pH 7.4) and calibrated with gel filtration molecular mass standards (12 to 200 kDa) (Sigma, St. Louis, MO). Eluted fractions (3 ml) were analyzed for P19 and TBSV siRNAs using Western and Northern blotting, respectively (see below). The protein content present in fractions was estimated with a Bio-Rad protein assay kit by a modification of the Bradford procedure (3). Relative band densities of the protein blots were determined using NIH image software http://rsb.info.nih.gov/nih-image/.

Ion-exchange chromatography. Twenty grams of infected *N. benthamiana* leaf tissue was homogenized in loading buffer (50 mM potassium phosphate pH 7.4, 5 mM DTT). The extract was filtered through cheesecloth and then centrifuged for 15 min at 14,000 × *g* at 4°C. The supernatant (20 ml) was loaded onto a 10-by 2.5-cm column packed with Marco-Prep DEAE Support (Bio-Rad, Hercules, CA). The column was washed with 100 ml of loading buffer, and the bound proteins were subsequently eluted with a gradient of increasing concentrations of NaCl (0.1 to 0.9 M). Every other fraction (2 ml) was analyzed for the presence of P19 protein and siRNAs.

Immunoprecipitation. For immunoprecipitation (IP), immediately after harvesting, 1 g of leaf tissue was pulverized in an ice-cold mortar with 1.5 ml of ice-cold extraction buffer: 150 mM HEPES (pH 7.5), 200 mM NaCl, 1 mM EDTA, 2 mM DTT, and protease inhibitor cocktail (Roche Diagnostics). The homogenized plant material was filtered through cheesecloth and centrifuged twice at 10,000 × *g* at 4°C for 15 min. An aliquot of 800 µl of the supernatant was mixed with 2 µl of TBSV P19 rabbit polyclonal antibodies and rotated for 2 h at 4°C. Then 30 µl of ImmunoPure Immobilized protein G agarose beads (Pierce, Rockford, IL) was added and the samples were incubated for an additional 2 h at room temperature. The beads were washed six times with ice-cold extraction buffer, and the precipitated material was analyzed by SDS-polyacrylamide gel electrophoresis (SDS-PAGE) followed by Western blot assays. To reduce the background noise on Western blots caused by cross-reaction between primary and secondary antibodies, TBSV P19 mouse polyclonal antibodies were used for protein detection.

Detection of TBSV siRNAs. To dissociate siRNAs from protein complexes in the fractions obtained by gel filtration, ion-exchange chromatography (350 µl), and immunoprecipitation (protein G agarose beads, 20 µl), samples were treated with 10% SDS (50 µl) at 65°C for 15 min, followed by phenol-chloroform extraction. RNA was then precipitated with 2.5 volumes of 100% ethanol and separated in 17% acrylamide gels in presence of 8 M urea, followed by electroblotting onto nylon membranes (Osmonics, Westborough, MA). TBSV-specific siRNAs were detected by hybridization with [^{32}P]dCTP-labeled TBSV-specific probes at 47°C followed by autoradiography. As a nucleotide size marker, the Decade Marker system (Ambion, Austin, TX) was used in the experiments.

Western blot analysis. Protein samples were separated by SDS-PAGE in 12% polyacrylamide gels and transferred to nitrocellulose membranes (Osmonics, Westborough, MA). After transfer, the membranes were stained with Ponceau S (Sigma, St. Louis, MO) to verify protein transfer efficiency. The dilution of the primary P19 antibodies was 1:5,000. Alkaline phosphatase conjugated to goat anti-mouse antiserum (Sigma) was used as a secondary antibody at a dilution of 1:1,000, and the immune complexes were visualized by hydrolysis of tetrazolium-5-bromo-4-chloro-3-indolyl phosphate as the substrate. In some experiments, horseradish peroxidase conjugated to goat anti-mouse antiserum (Bio-Rad, Hercules, CA) was used as a secondary antibody at a dilution of 1:5,000 and the immune complexes were visualized with an enhanced chemiluminescence detection kit (Pierce, Rockford, IL).

RESULTS

Coimmunoprecipitation of P19-siRNA complexes unexpectedly fails to confirm a strict correlation between siRNA binding and suppressor activity. Crucial biochemical properties that would determine the functionality of P19 are its early and abundant accumulation (12, 28), its capacity to form dimers (22), and the proper structural positioning of key amino acids to allow precise measuring and binding of siRNA (37, 42). To compare wtP19, P19/75-78, and P19/43 with regard to P19 accumulation and siRNA binding, we infected *N. benthamiana* plants with the corresponding viruses. Infection of *N. benthamiana* plants with wild-type TBSV resulted in typical severe symptoms on inoculated and upper leaves starting at 5 days postinoculation (dpi), rapidly followed by apical necrosis and systemic collapse (Fig. 1A). Symptoms on plants inoculated with transcripts of *p19* mutants either devoid of P19 expression (ΔP19) or expressing P19/75-78 (RR75-78GG) initially resembled those observed for wild-type TBSV. However, rather than succumbing to a lethal necrosis, the plants progressed to a recovery phenotype with mild symptoms on inoculated leaves and some leaf curling and mosaic in upper leaves (Fig. 1A). (Note that the phenotype for P19/75-78 was comparable to that shown for ΔP19.) Symptoms associated with P19/43 were intermediate: no lethal necrosis developed, but plants remained stunted (Fig. 1A).

Despite the milder symptoms, all mutants established a systemic infection, which is consistent with earlier findings that these mutants initially accumulate to similar levels in *N. benthamiana* (5). IP with P19-specific antiserum using *N. benthamiana* extracts confirmed that healthy plants and those infected with TBSV not expressing P19 (ΔP19) did not yield P19 (Fig. 1B). The pull-down procedure of samples extracted from plants
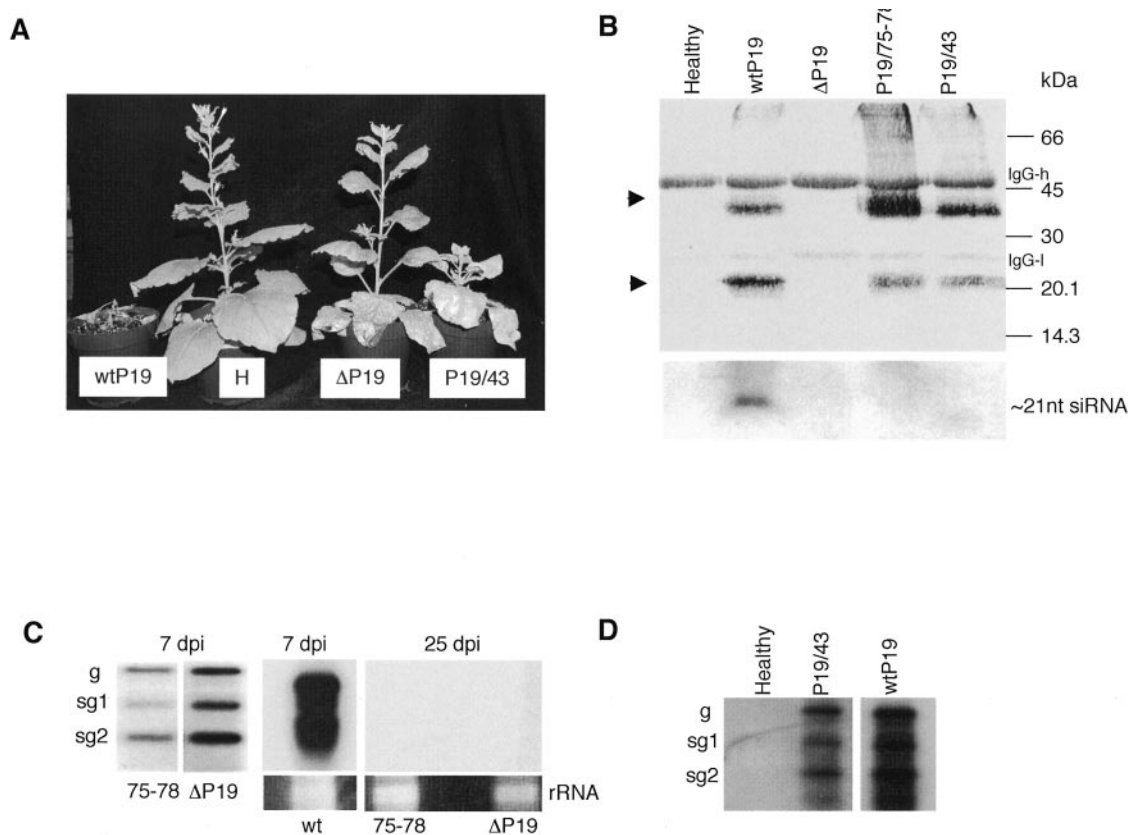
FIG. 1. Analysis of P19 with regards to a correlation between coimmunoprecipitating siRNAs and suppression of viral RNA degradation. (A) *N. benthamiana* plants inoculated with transcripts of TBSV expressing wtP19, no P19 (ΔP19), or P19/43, shown at 3 weeks postinoculation. H, healthy. (B) (Top panel) Western blot of P19 immunoprecipitated material obtained from healthy and infected plants at 5 days postinoculation. Although P19 was immunoprecipitated with P19-specific rabbit antibodies and P19 mouse antibodies were used as primary antiserum for Western blot detection, the cross-reaction of rabbit IgG heavy (h) and light (l) chains with the secondary anti-mouse antibody remains detectable. Arrowheads on the left side of the panel indicate positions of P19 monomers and dimers. Molecular mass markers in kDa are indicated on the right side of the panel. The total integral densities of P19 for wtP19, P19/75-78, and P19/43 (monomer plus dimer) were 0.152, 0.263, and 0.140 arbitrary units, respectively. (Bottom panel) Northern analysis for detection of TBSV-specific siRNAs using a TBSV-cDNA hybridization probe. (C) Total RNA collected from infected *N. benthamiana* at 7 or 25 dpi with TBSV ΔP19 or P19/75-78 was hybridized with a TBSV-specific probe to detect genomic RNA (g) and the two subgenomic RNAs (sg1 and sg2). The data aim to be qualitative: due to different exposures, no quantitative comparison is valid between the wild type at 7 dpi on the one hand and the P19/75-78 and ΔP19 mutants on the other (see reference 5 for a comparative study). The ethidium bromide-stained gel on the bottom of the right panel shows equal loading of rRNAs prior to transfer. (D) RNA collected from *N. benthamiana* at 21 dpi with TBSV P19/43. Since wild-type-inoculated plants have died at 21 dpi, that lane is from ~7 dpi.

infected with mutants expressing wtP19, P19/75-78, and P19/43 resulted in efficient precipitation of P19 that was detected as monomers and dimers upon Western blot analysis (Fig. 1B). It is important to note that in this experiment as in all other related experiments in this report, and as we reported previously (5, 22, 28, 35), even though the protein sample is denatured with SDS, a significant proportion of P19 dimers is recalcitrant to dissociation, and thus dimers often remain prominently visible upon SDS-PAGE.

When the IP samples were subsequently analyzed for siRNA content, only wtP19 was found to be associated with TBSV-specific ~21-nt siRNAs (Fig. 1B). The absence of siRNA association with P19/75-78 correlates with the finding that *N. benthamiana* plants infected with the cognate virus recover from the severe symptoms (5), corresponding to clearance of viral RNA (Fig. 1C). This is similar to what occurs for a mutant devoid of P19 expression (Fig. 1C) as also reported by others (24, 34); in fact, for unknown reasons, the clearance is often

more effective for P19/75-78 than for ΔP19 (data not shown). In contrast, the absence of ~21-nt TBSV siRNAs for P19/43 was unexpected because this mutant protein suppresses posttranscriptional silencing of a transgene (23), and here we verify that it is a functional suppressor for maintenance of TBSV RNA in infected *N. benthamiana* (Fig. 1D).

The loss of siRNA appropriation by P19/75-78 could either be due to a structural shift that could preclude proper dimer formation or to a specific RNA binding defect. To address this question and to further investigate the seeming paradox that loss of siRNA binding by P19/43 does not abolish its suppressor activity, further refined biochemical analyses were performed, as described below.

P19/75-78 forms dimers that are specifically compromised for siRNA binding, which is responsible for an irreversible recovery phenotype. Extracts from *N. benthamiana* plants infected with wild-type TBSV were fractionated by gel filtration chromatography through a Sephacryl S-200 HR column fol-
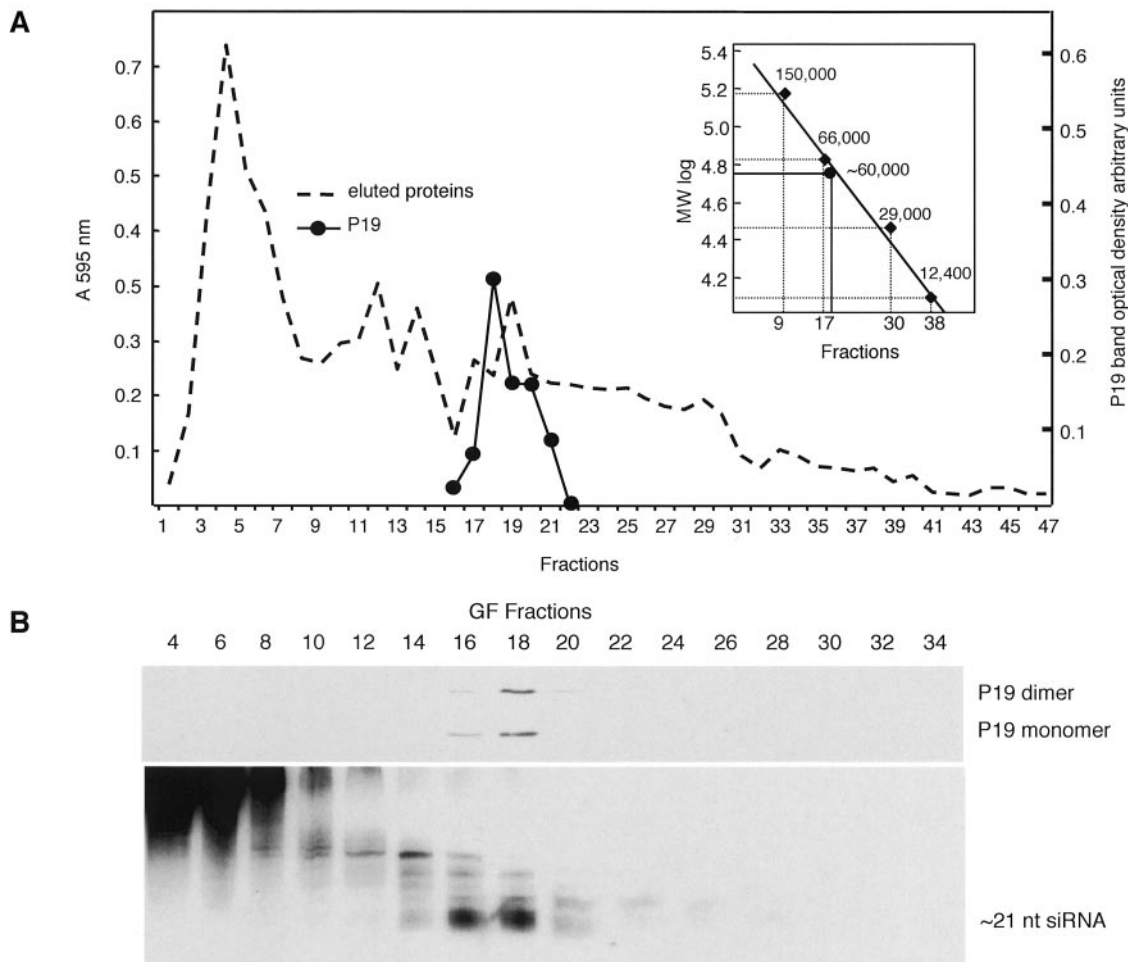
FIG. 2. Gel filtration chromatography with wild-type TBSV-infected *N. benthamiana* extracts on a Sephacryl S-200 HR column. (A) The dashed line provides the protein concentration in fractions (bottom) based on absorption at 595 nm (A 595; left axis). The solid line illustrates the relative concentration of the P19 complex, as measured in each fraction (dots) based on band intensity on Western blot analysis given in arbitrary units (right axis). The insert diagram represents column calibration with molecular mass standards and estimation of molecular mass of the eluted P19 complex ($\sim$60 kDa; dot connected to vertical and horizontal solid lines). TBSV-infected *N. benthamiana* leaves were collected for analysis at 4 dpi. (B) Western (top) and Northern (bottom) blot analyses of fractions (as in panel A) for detection of P19 and TBSV-specific siRNAs, respectively.

lowed by quantitative Western blot analyses for detection of P19 in individual fractions (Fig. 2A). These tests showed elution of wtP19 predominantly in fraction 18 ($\sim$54-ml elution volume) and equilibration of the column with standard molecular mass markers revealed that wtP19 eluted as a complex with a molecular mass of around 60 kDa (Fig. 2A). Northern blot analyses following denaturation gel electrophoresis showed that these fractions contained TBSV-specific siRNAs, as illustrated for the peak fraction 18 in Fig. 2B. These experiments confirm the results obtained with co-IP experiments (Fig. 1A) that TBSV-specific siRNAs are associated with wtP19. We did not observe detectable elution levels of momomeric P19, nor were 21-nt TBSV siRNAs detected in fractions not containing wtP19 (Fig. 2B). However, longer TBSV RNAs were present in other fractions, most notably in high-molecular-mass fractions, and siRNAs of slightly larger size than 21 nt also coeluted with P19 (Fig. 2B). Nevertheless, the observations are in accordance with the interpretation that virtually all circulating 21-nt TBSV-siRNAs are appropriated by P19 in planta.

Analyses of each 3-ml gel filtration sample (fractions 17 to 26) collected from plants infected with TBSV expressing P19/75-78 showed that this mutant P19 predominantly eluted in a higher volume than wtP19 (indicating a smaller Stokes radius of the complex) (Fig. 3A). Gel filtration with extracts from plants infected with viral RNAs expressing both wtP19 and P19/75-78 also resulted in two separate P19 elution peaks (Fig. 3A), confirming that the differences were not due to variability in chromatography conditions. The elution profile of P19/75-78 was reminiscent of what we observed previously for purified siRNA-free wtP19 that formed dimers in solution (22). These properties suggested that P19/75-78 was not present as an $\sim$19-kDa monomer in infected plants but instead formed dimers that were incapable of capturing siRNA. This interpretation was confirmed by Northern hybridization tests showing that the P19/75-78 peak fraction did not contain TBSV-specific 21-nt siRNAs (Fig. 3B). Therefore, combined with the IP data, we conclude that P19/75-78 forms dimers that are unable to associate with siRNAs during infection.

A

GF Fractions

17 18 19 20 21 22 23 24 25 26

wtP19

P19/75-78

wtP19+
P19/75-78

B

wtP19 P19/75-78 M nt

— 50
— 40

— 30

— 20

C

Superinoculation

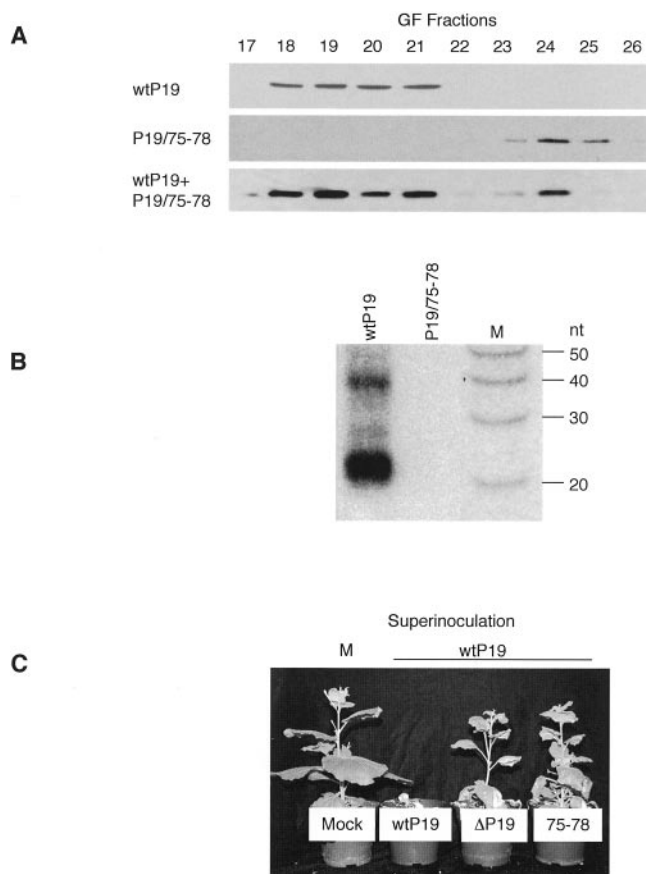M wtP19

Mock wtP19 ΔP19 75-78

FIG. 3. Properties of P19/75-78. (A) Western analyses for detection of P19 in fractions collected upon Sephacryl S-200 HR gel filtration chromatography with extracts from *N. benthamiana* plants infected with TBSV expressing either P19/75-78, wtP19, or both. Mouse P19 antiserum was used for protein detection, and the immune complexes were visualized by enhanced chemiluminescence. (B) Northern blot analysis of elution peak P19 fractions obtained from panel A (fraction 18 for wtP19 and fraction 24 for P19/75-78) for detection of TBSV-specific siRNAs. RNA molecular size markers and respective size in nucleotides are indicated on the rightmost side of the blot. *N. benthamiana* leaves were collected for analysis at 4 dpi. (C) *N. benthamiana* plants preinoculated with viral RNA expressing either wtP19, no P19 (ΔP19), or P19/75-78 were superinoculated 2 days later with RNA expressing wtP19 or mock inoculated (M). Photographs were taken 10 days after the second inoculation.

A

GF Fractions

15 16 17 18 19 20 21

P19/43 dimer

P19/43 monomer

~21 nt siRNA

B

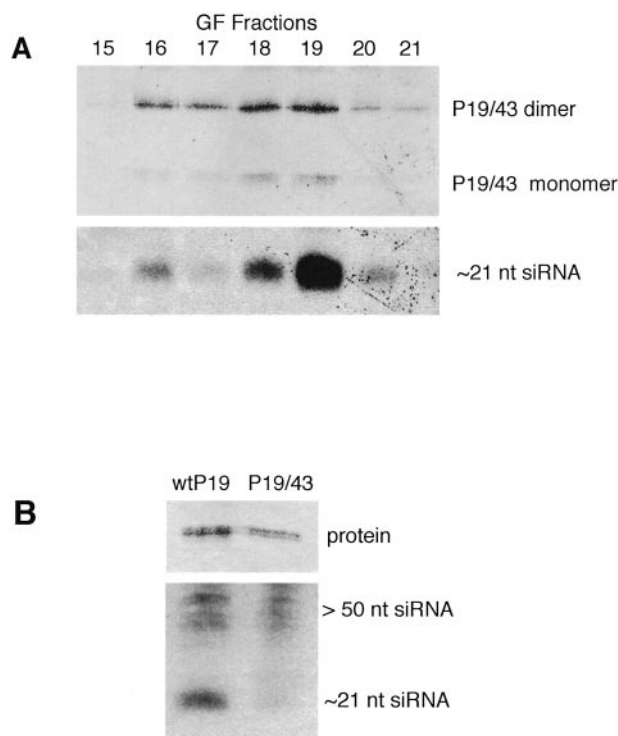wtP19 P19/43

protein

> 50 nt siRNA

~21 nt siRNA

FIG. 4. Properties of P19/43. (A) Fractions were collected upon gel filtration of extracts from *N. benthamiana* plants infected with the TBSV mutant expressing P19/43. The upper panel represents P19 protein detected by Western blot analysis on selected fractions. The bottom panel shows TBSV siRNAs detected in the same fractions by RNA hybridization. (B) Gel filtration elution peak fractions (as in Fig. 2 or as in panel A) containing wtP19 or P19/43 were subjected to P19-specific IP. The protein (Western) blot on top shows the comparable yield of wtP19 and P19/43 upon IP. The same samples were subsequently used for hybridization tests for detection of TBSV-specific siRNAs. The longer siRNAs of >50 nt were not detected upon co-IP with extracts from healthy plants or from plants infected with the mutant not expressing P19 (data not shown).

The biological implication of the above findings is that during infection of *N. benthamiana* with TBSV expressing P19/75-78, suppression of RNAi fails because the mutant protein does not appropriate siRNAs and thus these are available to program RISC. This model suggests that once anti-TBSV RISC becomes activated due to a faltering P19, the process cannot be reversed. To test this model, we superinoculated TBSV expressing wtP19 onto plants already inoculated 2 days previously with mutants either devoid of P19 expression (ΔP19) or expressing P19/75-78. Initially wtP19 accumulated to detectable levels in these doubly infected leaves (Fig. 3A). However, the plants did not succumb to a systemic collapse otherwise induced by wtP19 (Fig. 3C). Instead the plants progressed to the recovery phenotype, suggesting that systemic RISC pro-

gramming had occurred, thus preventing wild-type TBSV from causing a lethal infection.

The binding of 21-nt siRNAs by P19/43 dimers depends on the surrounding ionic strength. The elution characteristics of P19/43 upon gel fractionation were similar to those of wtP19, with a predominant peak in fractions 17 to 21 and the association with ~21- to 25-nt TBSV-specific siRNAs (Fig. 4A). These data show that P19/43 forms dimers that have the capacity to bind siRNAs in infected plants, which at first sight seems to conflict with the co-IP data (Fig. 1B). However, the co-IP experiments were performed in the presence of salt, which is absent during gel filtration. This observation combined with the position of the substitute Trp in P19/43 (elaborated on in the Discussion) led us to hypothesize that the interaction between P19/43 and siRNAs may be governed by electrostatic interactions that are less robust than those that occur for wtP19 and thus susceptible to the presence of NaCl. To test this, we performed co-IP experiments on P19-siRNA enriched gel filtration fractions for wtP19 and P19/43 in the presence of 50 mM NaCl and subjected the pulled-down material to Northern blot hybridization. The results show similar
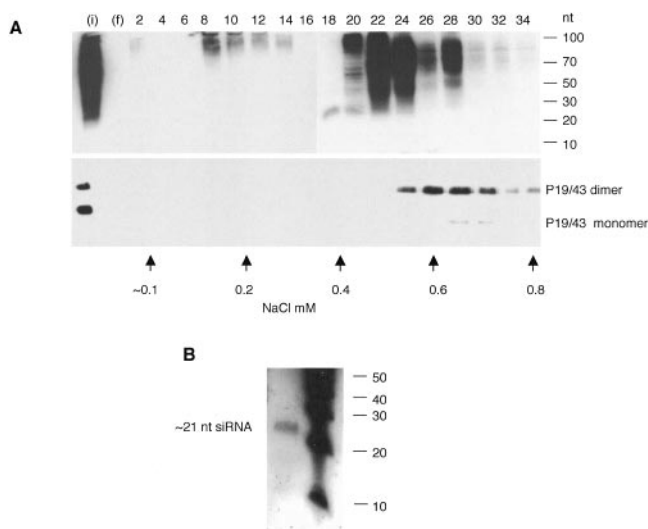
FIG. 5. Ionic strength-related siRNA binding properties of P19/43. (A) (Top) Northern blot hybridization for detection of short (<100 nt) TBSV-specific RNAs in fractions collected upon DEAE ion-exchange chromatography with extracts from *N. benthamiana* plants infected with the TBSV mutant expressing P19/43. The positions of RNA molecular mass markers are indicated on the rightmost side of the blot. Numbers on the top indicate order of fractions for both panels. Numbers and arrows on the bottom indicate the linear gradient of NaCl concentration from 0.1 to 0.8 mM. Input and flowthrough are indicated as (i) and (f), respectively. (Bottom) Western blot assay for detection of P19 in DEAE-eluted fractions. Mouse P19 antiserum was used for protein detection, and immune complexes were visualized by chemiluminescence detection. In this experiment, P19/43 remained mostly present as a dimer during SDS-PAGE. Note that ~21-nt siRNAs are not associated with P19/43 but instead elute with fractions 18 to 20. *N. benthamiana* leaves were collected for analysis at 4 dpi. (B) siRNAs extracted from fraction 18 depicted next to RNA molecular mass markers.

levels of P19, yet the amount of 21-nt siRNAs associated with P19/43 was now substantially reduced (Fig. 4B). This illustrates that siRNAs dissociate from P19/43 in the presence of exogenously added NaCl, whereas similar conditions do not affect the siRNA association with wtP19. These experiments should also serve as a general cautionary note that co-IP experiments should be verified by independent methods.

The Northern blots in Fig. 2, 3, and 4 (and data not shown) illustrate that wtP19 and P19/43 not only bind ~21-nt siRNAs but also bind TBSV-specific RNAs of larger molecular mass. These may represent siRNA precursors, and the binding of these molecules to P19/43 appears less severely compromised by addition of salt than the effect observed for the 21-nt siRNAs (Fig. 4B). To further investigate the difference in NaCl sensitivity of P19/43 for different sized siRNAs, we performed ion-exchange chromatography with extracts from plants infected with virus expressing P19/43, whereby material is eluted from the DEAE support by a gradient of increasing NaCl concentration. These experiments revealed the presence of a broad spectrum of >21- to 100-nt TBSV RNAs (Fig. 5A). In addition, the same fractions exhibited an abundant level of long TBSV dsRNAs (not shown). Despite the coelution of larger RNAs with P19/43, the ~21-nt siRNAs were predominantly present in fractions 18 to 20, which lack the P19/43 protein (Fig. 5A and B).

In support of this observation, the DEAE fractionation of plant material infected with P19/157 (ΔP19) resulted in the elution profile of the 21-nt siRNAs that is identical to that observed for P19/43 (not shown). Thus, the P19/43-siRNA interaction is susceptible to the presence of NaCl, whereas the interaction with longer siRNAs (that coelute with P19/43, Fig. 5) appears less affected by the ionic strength of the surrounding solution. These data suggest that even though the 21-nt siRNA binding capacity by P19/43 is altered, the remaining affinity, perhaps together with the unaltered ability to bind longer siRNAs, is sufficient to suppress gene silencing (Fig. 1D) (23). However, *N. benthamiana* plants infected with virus expressing P19/43 have an intermediate symptom phenotype compared to that observed for plants infected with TBSV expressing wtP19 versus those infected in absence of P19 (Fig. 1A).

In summary, the biochemical tests show that in TBSV-infected plants, (i) wtP19 dimers appropriate the circulating virus-specific siRNAs, (ii) P19/75-78 and P19/43 accumulate to levels comparable to those observed for wtP19, (iii) the mutants form dimers in planta, (iv) P19/75-78 is defective for siRNA binding, and (v) P19/43 is somewhat destabilized for the interaction with ~21-nt siRNAs but not for interaction with longer siRNAs.

DISCUSSION

The *Tombusvirus*-encoded suppressor of RNA silencing P19 forms dimers that bind siRNAs in vitro and in vivo (10, 12, 37, 42). Although mutagenesis of the siRNA-bordering P19 caliper tryptophan residues was shown to have an effect on virus-induced symptoms (37), in this study we provide the first clear evidence for a direct link between the biochemical affinity of P19 for siRNAs and its subsequent biological role in maintenance of viral RNA (i.e., suppression of RNA silencing) and viral pathogenicity.

We demonstrate that the previously observed *p19*-null-mimicking phenotype observed for plants infected with TBSV expressing P19/75-78 (5, 35) correlates with its inability to prevent viral RNA degradation. We show that the initial accumulation of P19/75-78 is comparable to that observed for wtP19 and that P19/75-78 has retained the intrinsic capacity to form dimers. Using independent biochemical methods, conclusive evidence is provided that P19/75-78 dimers are specifically compromised to bind TBSV-specific siRNAs in planta. The analysis of the crystallographic structure of the P19-siRNA complex does not support a direct role of the Arg residues at positions 75 and 78 as contact points with siRNA. However Arg at position 75 and Glu at position 41 may form an interface salt bridge between the N-terminal and C-terminal subdomains that is suggested to be involved in the proper positioning of the caliper tryptophan residues for binding of siRNAs (37). This suggests that the mutation in P19/75-78 prohibits the formation of this essential salt bridge and thus causes a slight structural change that prevents the binding of the siRNAs.

The results obtained with P19/75-78 support the notion that the ability of P19 to bind siRNAs is crucial for its function as a suppressor of RNA silencing in *N. benthamiana*. Whether these P19-bound siRNAs are subsequently sequestered for turnover, perhaps by mediation of host RNA processing factors (22, 36), remains to be determined. Regardless, since TBSV can give
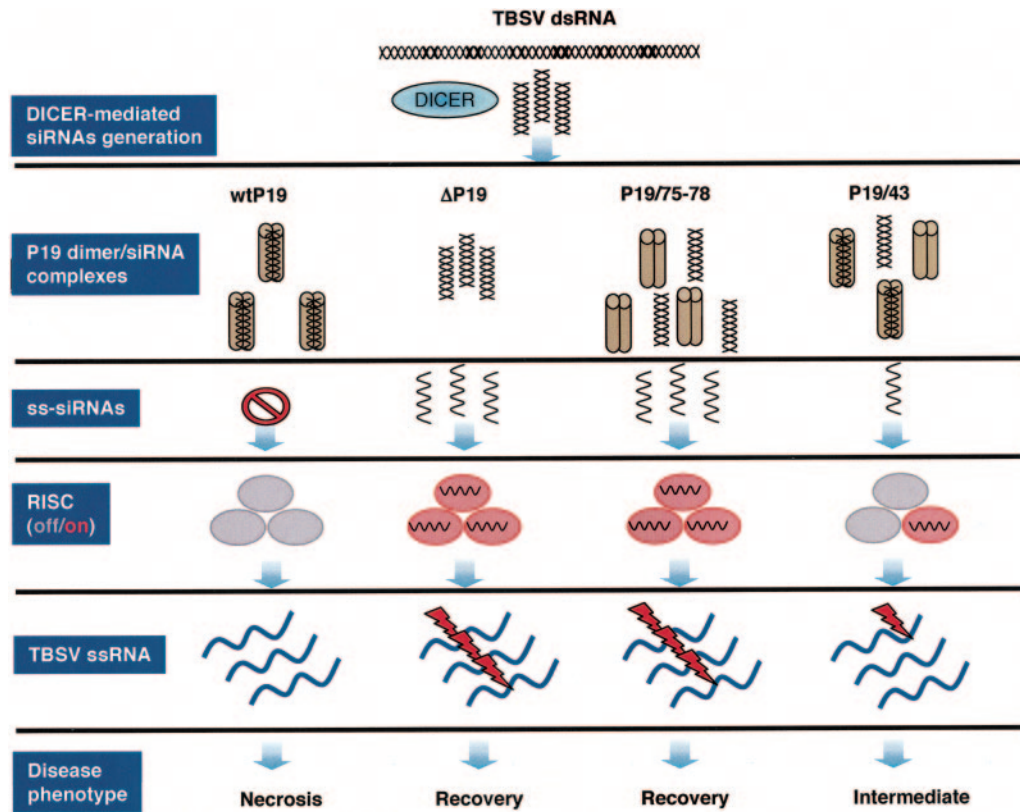
FIG. 6. Schematic model of the effects of P19 mutations on TBSV infections of *N. benthamiana*. Long TBSV dsRNAs are cleaved by Dicer to generate double-stranded siRNAs (~21 bp), which are then unwound for incorporation into RISC. Programmed RISCs recognize their targets (TBSV ssRNAs) and direct RNA degradation. In the case of infections with TBSV expressing wtP19, siRNA duplexes are appropriated to prevent their unwinding and subsequent incorporation into RISC. In the case of defective P19 mutants, siRNAs are transferred to RISC to cause virus RNA degradation and altered disease symptoms.

rise to high levels of siRNAs (data not shown), in hindsight the crucial role for siRNA sequestration by P19 is also in agreement with our previous results that P19 is rapidly accumulating at early stages and only functional when produced at high levels (23, 28). The implication is that in plant cells there is a constitutive amount of RISC available that is ready for instantaneous activation by siRNAs (Fig. 6). However, wtP19 blocks this activation, whereas the compromised ability of P19/75-78 to bind siRNAs results in the transfer of siRNAs from Dicer to RISC, which subsequently becomes programmed for destruction of viral RNA to result in reduction of viral load, impaired systemic invasion, and recovery (Fig. 6). In addition, our cross-inoculation experiments indicate that the integration of siRNAs into the RISC nuclease complex cannot be reversed by P19: in other words, P19 is unable to deprogram RISC. This agrees with previous observations that P19 was not able to reverse posttranscriptional transgene silencing in tissues in which this process was already firmly established (23, 25, 39). Conversely, superinoculation of the mutant ΔP19 or P19/75-78 onto plants already infected 2 days earlier with wild-type TBSV does not lead to recovery (data not shown). In accordance with the model (Fig. 6), the presence of wt P19 in these plants prevents the activation of RISC by the mutants.

Previously, we also reported on another P19 mutant (P19/71-72) that was essentially inactive for all P19-mediated activ-

ities (5, 22, 35), and others have recreated this mutant to serve as a negative control during RNAi studies (6). However, the lack of self-interaction of this mutant in yeast two-hybrid studies (22) and recently observed unusual chromatography elution properties (not shown) illustrate that the P19/71-72 protein is not a suitable control candidate. For that purpose, we suggest that P19/75-78 should be used in future RNAi studies.

In earlier studies, we also demonstrated that P19/43 has a pathogenicity phenotype for host-dependent spread and symptom induction that is "intermediate" compared with those of TBSV infections mediated by wtP19 versus those that occur in the absence of P19 (5, 35), and as shown in Fig. 1A. The substitute Trp43 in P19/43 is adjacent to Trp42, which forms one of the calipers important for siRNA binding (37). This raised the possibility that the mutation in P19/43 interferes with, but does not abolish, siRNA binding, providing a biochemical explanation for its intermediate phenotypic behavior. To test this hypothesis, we analyzed P19/43 for its ability to prevent TBSV degradation and to bind siRNAs. The results show that P19/43 is able to suppress silencing-mediated degradation of TBSV RNA that remains detectable weeks after infection, at which time plants infected with wild-type TBSV have long died. These results agree with our previous finding that P19/43 suppresses virus-induced degradation of transgenic green fluorescent protein (GFP) expression (23). Gel-filtration

chromatography and subsequent analyses verified that P19/43 binds TBSV-derived siRNAs. However, ion-exchange chromatography and co-IP methods that both involve the use of NaCl resulted in P19/43 products that, unlike wtP19, are no longer associated with ~21-nt siRNAs, although longer siRNAs remained bound to the protein. These longer molecules could represent precursors of the 21-nt siRNAs, and thus P19 might be present in close association with DICER in the cell. Collectively, the results strongly suggest that the wtP19 dimer is structurally finely tuned for optimum and stable electrostatic interaction with 21-nt siRNAs, whereas the binding of longer possible progenitor siRNAs may be less confined.

Our data obtained with P19/43 agree with electrostatic properties that were inferred from the structural analysis of the P19-siRNA complex (37, 42). At each end of the P19 dimer, the Trp42 caliper of the individual monomers forms a hydrogen bond with the 5′-phosphorylated duplex siRNA. The adjacent Arg43 (substituted for Trp in P19/43) is conserved among tombusviruses, and its structural role is to stack with the other caliper Trp39, to prevent the surface exposure of this hydrophobic residue. The substitution of Arg43 for Trp may thus interfere with the establishment of a hydrogen bond with the 5′ phosphate of the 21-nt siRNA or cause inappropriate surface exposure of regulatory hydrophobic residues. This apparently results in NaCl-sensitive binding of the 21-nt siRNAs. This suggests that, compared to wtP19, P19/43 is more susceptible to dissociation of 21-nt siRNA, and this may cause "leaky" programming of RISC, and thus an intermediate phenotype ensues (Fig. 6). This agrees with preliminary gel filtration results with extracts from plants infected with TBSV-P19/43 that revealed the presence of single-stranded TBSV-specific siRNAs in high-molecular-mass fractions that possess RISC-like activity (R. Omarov and H. B. Scholthof, unpublished observations).

A biological ramification is that even though P19/43 suppresses RNA silencing, it does not cause P19-associated lethal necrotic symptoms on *N. benthamiana* (Fig. 1A) or a hypersensitive defense response on *Nicotiana tabacum* (5). Others have proposed that symptoms caused by expression of suppressors may be related to their interference with microRNA (miRNA) function (4, 21). However, the initial mosaic and systemic leaf curl symptoms that occur on *N. benthamiana* upon TBSV infection are also apparent in the absence of P19 (5, 31; data not shown). Furthermore, our results show that both wtP19 and P19/43 bind 21-nt siRNAs and suppress RNA silencing, but unlike wtP19, P19/43 does not cause a lethal necrosis. This suggests that the differences regarding the severity of symptoms might be related either to a diminished affinity of P19/43 for miRNAs or to roles of P19 in addition to the siRNA (or miRNA) binding. Along the same lines, in contrast to the dispensability of P19 for initial systemic invasion of *N. benthamiana*, P19 is required for spread through inoculated leaves of pepper (31). This would readily lead to the interpretation that siRNA binding by P19 is important for local movement in this host. Yet, P19/75-78 is functional for local spread in pepper (35), even though it fails to appropriate siRNAs. Thus, it seems that P19 may perform additional roles unrelated to siRNA binding to promote movement through inoculated pepper leaves. This is entirely in agreement with our observations over the years that the role of P19 is host specific (5, 28, 30, 31, 35). Thus, siRNA binding is a key

property for systemic TBSV invasion of plants, and other host-dependent features contribute to this process.

In conclusion, we have shown that the role of P19 to prevent degradation of its cognate viral genome in infected *N. benthamiana* plants correlates with its structurally governed ability to stably bind TBSV-derived siRNAs. In combination with our previous observations that the P19-mediated activities for virus spread and silencing suppression depend on relatively high levels of its expression, the properties support the model (Fig. 6) that a central role of P19 during infection is to scavenge the abundant levels of TBSV-derived siRNAs. This avoids their loading into RISC to prevent viral RNA degradation, which permits the establishment and maintenance of a systemic infection. The findings should be of broad interest to the RNAi field in general because the implementation of our mutant P19 proteins provides the unique ability to precisely control siRNA transfer between Dicer and RISC in several model systems.

REFERENCES

1. **Baulcombe, D.** 1999. Viruses and gene silencing in plants. Arch. Virol. Suppl. **15:**189–201.
2. **Bernstein, E., A. A. Caudy, S. M. Hammond, and G. J. Hannon.** 2001. Role for a bidentate ribonuclease in the initiation step of RNA interference. Nature **409:**363–366.
3. **Bradford, M. M.** 1976. A rapid and sensitive method for the quantitation of microgram quantities of protein utilizing the principle of protein-dye binding. Anal. Biochem. **72:**248–254.
4. **Chapman, E. J., A. I. Prokhnevsky, K. Gopinath, V. V. Dolja, and J. C. Carrington.** 2004. Viral RNA silencing suppressors inhibit the microRNA pathway at an intermediate step. Genes Dev. **18:**1179–1186.
5. **Chu, M., B. Desvoyes, M. Turina, R. Noad, and H. B. Scholthof.** 2000. Genetic dissection of tomato bushy stunt virus p19-protein-mediated host-dependent symptom induction and systemic invasion. Virology **266:**79–87.
6. **Dunoyer, P., C. H. Lecellier, E. A. Parizotto, C. Himber, and O. Voinnet.** 2004. Probing the microRNA and small interfering RNA pathways with virus-encoded suppressors of RNA silencing. Plant Cell **16:**1235–1250.
7. **Elbashir, S. M., W. Lendeckel, and T. Tuschl.** 2001. RNA interference is mediated by 21- and 22-nucleotide RNAs. Genes Dev. **15:**188–200.
8. **Filipowicz, W.** 2005. RNAi: the nuts and bolts of the RISC machine. Cell **122:**17–20.
9. **Hammond, S. M., S. Boettcher, A. A. Caudy, R. Kobayashi, and G. J. Hannon.** 2001. Argonaute2, a link between genetic and biochemical analyses of RNAi. Science **293:**1146–1150.
10. **Havelda, Z., C. Hornyik, A. Válóczi, and J. Burgyán.** 2005. Defective interfering RNA hinders the activity of a tombusvirus-encoded posttranscriptional gene silencing suppressor. J. Virol. **79:**450–457.
11. **Hearne, P. Q., D. A. Knorr, B. I. Hillman, and T. J. Morris.** 1990. The complete genome structure and synthesis of infectious RNA from clones of tomato bushy stunt virus. Virology **177:**141–151.
12. **Lakatos, L., G. Szittya, D. Silhavy, and J. Burgyan.** 2004. Molecular mechanism of RNA silencing suppression mediated by p19 protein of tombusviruses. EMBO J. **23:**876–884.
13. **Lecellier, C. H., P. Dunoyer, K. Arar, J. Lehmann-Che, S. Eyquem, C. Himber, A. Saib, and O. Voinnet.** 2005. A cellular microRNA mediates antiviral defense in human cells. Science **308:**557–560.
14. **Liu, J. D., M. A. Carmell, F. V. Rivas, C. G. Marsden, J. M. Thomson, J. J. Song, S. M. Hammond, L. Joshua-Tor, and G. J. Hannon.** 2004. Argonaute2 is the catalytic engine of mammalian RNAi. Science **305:**1437–1441.
15. **Mallory, A. C., B. J. Reinhart, D. Bartel, V. B. Vance, and L. H. Bowman.** 2002. A viral suppressor of RNA silencing differentially regulates the accumulation of short interfering RNAs and micro-RNAs in tobacco. Proc. Natl. Acad. Sci. USA **99:**15228–15233.
16. **Martinez, J., A. Patkaniowska, H. Urlaub, R. Luhrmann, and T. Tuschl.** 2002. Single-stranded antisense siRNAs guide target RNA cleavage in RNAi. Cell **110:**563–574.

17. Meister, G., M. Landthaler, A. Patkaniowska, Y. Dorsett, G. Teng, and T. Tuschl. 2004. Human Argonaute2 mediates RNA cleavage targeted by miRNAs and siRNAs. Mol. Cell. 15:185–197.

18. Molnár, A., T. Csorba, L. Lakatos, É. Várallyay, C. Lacomme, and J. Burgyán. 2005. Plant virus-derived small interfering RNAs originate predominantly from highly structured single-stranded viral RNAs. J. Virol. 79:7812–7818.

19. Myers, J. W., J. T. Jones, T. Meyer, and J. E. Ferrell. 2003. Recombinant Dicer efficiently converts large dsRNAs into siRNAs suitable for gene silencing. Nat. Biotechnol. 21:324–328.

20. Nykanen, A., B. Haley, and P. D. Zamore. 2001. ATP requirements and small interfering RNA structure in the RNA interference pathway. Cell 107:309–321.

21. Papp, I., M. F. Mette, W. Aufsatz, L. Daxinger, S. E. Schauer, A. Ray, J. van der Winden, M. Matzke, and A. J. Matzke. 2003. Evidence for nuclear processing of plant micro RNA and short interfering RNA precursors. Plant Physiol. 132:1382–1390.

22. Park, J. W., S. Faure-Rabasse, M. A. Robinson, B. Desvoyes, and H. B. Scholthof. 2004. The multifunctional plant viral suppressor of gene silencing P19 interacts with itself and an RNA binding host protein. Virology 323:49–58.

23. Qiu, W., J. W. Park, and H. B. Scholthof. 2002. Tombusvirus P19-mediated suppression of virus-induced gene silencing is controlled by genetic and dosage features that influence pathogenicity. Mol. Plant-Microbe Interact. 15:269–280.

24. Qu, F., and T. J. Morris. 2002. Efficient infection of Nicotiana benthamiana by Tomato bushy stunt virus is facilitated by the coat protein and maintained by p19 through suppression of gene silencing. Mol. Plant-Microbe Interact. 15:193–202.

25. Qu, F., T. Ren, and T. J. Morris. 2003. The coat protein of turnip crinkle virus suppresses posttranscriptional gene silencing at an early initiation step. J. Virol. 77:511–522.

26. Roth, B. M., G. J. Pruss, and V. B. Vance. 2004. Plant viral suppressors of RNA silencing. Virus Res. 102:97–108.

27. Scholthof, H. B. 2005. Plant virus transport: motions of functional equivalence. Trends Plant Sci. 10:376–382.

28. Scholthof, H. B., B. Desvoyes, J. Kuecker, and E. Whitehead. 1999. Biological activity of two tombusvirus proteins translated from nested genes is influenced by dosage control via context-dependent leaky scanning. Mol. Plant-Microbe Interact. 12:670–679.

29. Scholthof, H. B., T. J. Morris, and A. O. Jackson. 1993. The capsid protein gene of tomato bushy stunt virus is dispensable for systemic movement and can be replaced for localized expression of foreign genes. Mol. Plant-Microbe Interact. 6:309–322.

30. Scholthof, H. B., K. B. Scholthof, and A. O. Jackson. 1995. Identification of tomato bushy stunt virus host-specific symptom determinants by expression of individual genes from a potato virus X vector. Plant Cell 7:1157–1172.

31. Scholthof, H. B., K. B. Scholthof, M. Kikkert, and A. O. Jackson. 1995. Tomato bushy stunt virus spread is regulated by two nested genes that function in cell-to-cell movement and host-dependent systemic invasion. Virology 213:425–438.

32. Silhavy, D., and J. Burgyan. 2004. Effects and side-effects of viral RNA silencing suppressors on short RNAs. Trends Plant Sci. 9:76–83.

33. Silhavy, D., A. Molnar, A. Lucioli, G. Szittya, C. Hornyik, M. Tavazza, and J. Burgyan. 2002. A viral protein suppresses RNA silencing and binds silencing-generated, 21- to 25-nucleotide double-stranded RNAs. EMBO J. 21:3070–3080.

34. Szittya, G., A. Molnar, D. Silhavy, C. Hornyik, and J. Burgyan. 2002. Short defective interfering RNAs of tombusviruses are not targeted but trigger post-transcriptional gene silencing against their helper virus. Plant Cell 14:359–372.

35. Turina, M., R. Omarov, J. F. Murphy, C. Bazaldua-Hernandez, B. Desvoyes, and H. B. Scholthof. 2003. A newly identified role for Tomato bushy stunt virus P19 in short distance spread. Mol. Plant Pathol. 4:67–72.

36. Uhrig, J. F., T. Canto, D. Marshall, and S. A. MacFarlane. 2004. Relocalization of nuclear ALY proteins to the cytoplasm by the tomato bushy stunt virus P19 pathogenicity protein. Plant Physiol. 135:2411–2423.

37. Vargason, J. M., G. Szittya, J. Burgyan, and T. M. Tanaka Hall. 2003. Size selective recognition of siRNA by an RNA silencing suppressor. Cell 115:799–811.

38. Voinnet, O. 2005. Induction and suppression of RNA silencing: insights from viral infections. Nat. Rev. Genet. 6:206–220.

39. Voinnet, O., Y. M. Pinto, and D. C. Baulcombe. 1999. Suppression of gene silencing: a general strategy used by diverse DNA and RNA viruses of plants. Proc. Natl. Acad. Sci. USA 96:14147–14152.

40. Voinnet, O., S. Rivas, P. Mestre, and D. Baulcombe. 2003. An enhanced transient expression system in plants based on suppression of gene silencing by the p19 protein of tomato bushy stunt virus. Plant J. 33:949–956.

41. Yamamura, Y., and H. B. Scholthof. 2005. Tomato bushy stunt virus: a resilient model system to study virus-plant interactions. Mol. Plant Pathol. 6:491–502.

42. Ye, K., L. Malinina, and D. J. Patel. 2003. Recognition of small interfering RNA by a viral suppressor of RNA silencing. Nature 426:874–878.

43. Zamore, P. D., T. Tuschl, P. A. Sharp, and D. P. Bartel. 2000. RNAi: double-stranded RNA directs the ATP-dependent cleavage of mRNA at 21 to 23 nucleotide intervals. Cell 101:25–33.